Autonomous Parameter Design for Cascade Structure Feedback Controller Based on Time and Frequency Domain Optimization

1st Eitaro Kuroda
Department of Electrical and Mechanical Engineering
Nagoya Institute of Technology
Nagoya, Japan
Email: e.kuroda.963@stn.nitech.ac.jp

2nd Yoshihiro Maeda
Department of Electrical and Mechanical Engineering
Nagoya Institute of Technology
Nagoya, Japan
Email: ymaeda@nitech.ac.jp

3rd Makoto Iwasaki
Department of Electrical and Mechanical Engineering
Nagoya Institute of Technology
Nagoya, Japan
Email: iwasaki@nitech.ac.jp

***Abstract*—This paper presents an autonomous parameter design method for a cascade structure feedback (FB) controller in industrial precision servo systems with resonance modes, considering a time and frequency domain optimization. In conventional autonomous design methods, parameters of a cascade structure FB controller are optimized by solving a frequency domain optimization problem to expand the control bandwidth and satisfy the desired stability margins. Therefore, a desired positioning response that is generally defined in time domain is not necessarily realized by the designed FB controller. The proposed method combines a time domain optimization problem to a conventional frequency domain optimization problem for improving the time domain positioning response. The effectiveness of the proposed method is demonstrated through an example FB controller design for a galvanometer scanner, in comparison with the conventional autonomous design method based on only the frequency domain parameter optimization.**

***Index Terms*—Autonomous parameter design, cascade structure, control bandwidth, control stability, feedback controller, time domain response**

I. Introduction

For realizing the fast response and high precision motion control of industrial servo systems, it is essential to design a proper feedback (FB) controller that achieves both desired frequency domain properties (e.g., control bandwidth and stability margins) and desired time domain properties (e.g. settling time and settling accuracy) [1], [2]. Especially, for servo systems with resonance modes, the gain/phase stabilization method is often utilized to design such a proper FB controller. In this method, multiple second-order filters (e.g., notch/all-pass filters) are commonly utilized for stabilizing resonance modes [3], [4]. In addition, a compensator for a rigid mode such as a PID compensator or a phase lead-lag compensator is connected with the filters, which forms cascade structure [5]. Although a cascade structure FB controller shows effective performance, researchers and industrial engineers needs to acquire high expertise to design all parameters of the FB controller when a target system has high-order resonance modes. Therefore, autonomous parameter design technique will be desired to easily obtain a high performance FB controller.

In recent years, there are some researches on autonomous parameter design methods based on numerical optimization techniques in literature, e.g., the structured H_∞ control [6], [7], the metaheuristics [8], [9], and the nonlinear optimization [10]. In these methods, the parameter optimization problem basically consists of an objective function for expanding the control bandwidth under a constraint for the stability margins on the frequency domain. Therefore, there is no guarantee that the designed FB controller achieves the desired time domain response. For designing proper FB controller parameters, the time domain properties should be also considered in the parameter optimization problem.

In this paper, an autonomous parameter design method for a cascade structure FB controller considering frequency and time domain properties is developed to obtain proper parameters. In the proposed method, a cooperative parameter optimization combining a sequential quadratic programming (SQP) and a genetic algorithm (GA) is utilized as basis for an autonomous parameter design method [11]. In the cooperative parameter optimization, linear parameters (e.g., PID gains) are optimized by the SQP based on the frequency domain optimization problem to stabilize FB control, while the remaining parameters (e.g., parameters of notch/all-pass filters) are optimized by the GA based on a newly developed time domain optimization problem to improve the position tracking performance. The effectiveness of the proposed method is demonstrated through an example FB controller design simulation for a galvanometer scanner, in comparison with the conventional cooperative parameter design method based on only the frequency domain parameter optimization.

II. Design Problem

Fig. 1 shows a block diagram of the two-degree-of-freedom (2-DoF) control system, where $C_{\mathrm{PID}}(s)$ is the PID compensator for rigid mode compensation, $C_{\mathrm{APF}}(s)$ is the all-pass filter for resonance mode compensation, $P(s)$ is the plant with resonance modes, r is the reference, e is the tracking error, u_{FB} is an FB control input, u_{FF} is an feedforward (FF) control

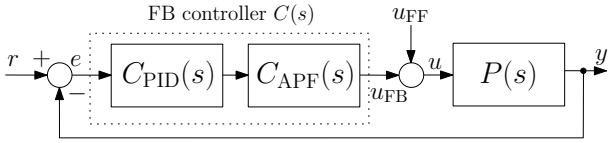

Fig. 1. Block diagram of the 2-DoF control system.

input, u is the control input and y is the controlled output. The compensators $C_{\mathrm{PID}}(s)$ and $C_{\mathrm{APF}}(s)$ are connected in series and form a cascade structure FB controller $C(s)$ defined as follows:

$$C(s) = C_{\mathrm{PID}}(s) \prod_{i=1}^{N_{\mathrm{A}}} C_{\mathrm{APF}}^{(i)}(s) \tag{1}$$

with

$$C_{\mathrm{PID}}(s) = K_{\mathrm{P}} + \frac{K_{\mathrm{I}}}{s} + \frac{K_{\mathrm{D}} s}{\tau_{\mathrm{D}} s + 1} \tag{2}$$

$$C_{\mathrm{APF}}^{(i)}(s) = \frac{s^2 - 2\zeta_{\mathrm{A}i}\omega_{\mathrm{A}i}s + \omega_{\mathrm{A}i}^2}{s^2 + 2\zeta_{\mathrm{A}i}\omega_{\mathrm{A}i}s + \omega_{\mathrm{A}i}^2} \tag{3}$$

where the number of all-pass filters is N_{A}. The purpose of this study is to autonomously design following parameters of $C(s)$ which satisfies the specified stability margin (i.e., gain margin of g_{m} [dB] and phase margin of ϕ_{m} [deg]) on the frequency domain and achieves the settling accuracy $\pm\varepsilon$ of the tracking error e or less to the reference r within the settling time T_{set} on the time domain.

$$\boldsymbol{\Lambda}_C = \left[K_{\mathrm{P}}\ K_{\mathrm{I}}\ K_{\mathrm{D}}\ \tau_{\mathrm{D}}\ \zeta_{\mathrm{A}\{1,\ldots,N_{\mathrm{A}}\}}\ \omega_{\mathrm{A}\{1,\ldots,N_{\mathrm{A}}\}}\right] \tag{4}$$

III. Autonomous Parameter Design Methods

A. Frequency Domain Optimization Method (Conventional)

In this section, a cooperative parameter design method [5], [11] based on the frequency domain parameter optimization is introduced as a conventional method.

1) Design Algorithm: Fig. 2 shows a flowchart of designing the controller parameters $\boldsymbol{\Lambda}_C$ based on the conventional autonomous design method. In Fig. 2, $\boldsymbol{\rho}_{\mathrm{SQP}}$ is a vector of PID parameters defined as (5) and satisfies (6) and (7).

$$\boldsymbol{\rho}_{\mathrm{SQP}} = \left[K_{\mathrm{P}}\ K_{\mathrm{I}}\ K_{\mathrm{D}}\right] \in \mathbb{R}^{1\times 3} \tag{5}$$

$$C(s) = \boldsymbol{\Psi}_{\mathrm{GA}}(s)\boldsymbol{\rho}_{\mathrm{SQP}}^{\top} \tag{6}$$

$$\boldsymbol{\Psi}_{\mathrm{GA}}(s) = C_{\mathrm{APF}}(s)\left[1\ \frac{1}{s}\ \frac{s}{\tau_{\mathrm{D}}s+1}\right] \in \mathbb{C}^{1\times 3} \tag{7}$$

On the other hand, $\boldsymbol{\rho}_{\mathrm{GA}}$ is a vector of the remaining parameters of $\boldsymbol{\Lambda}_C$ defined as (8).

$$\boldsymbol{\rho}_{\mathrm{GA}} = \left[\tau_{\mathrm{D}}\ \zeta_{\mathrm{APF}\{1,\ldots,N_{\mathrm{APF}}\}}\ \omega_{\mathrm{APF}\{1,\ldots,N_{\mathrm{APF}}\}}\right] \tag{8}$$

The cooperative optimization method optimize $\boldsymbol{\rho}_{\mathrm{SQP}}$ and $\boldsymbol{\rho}_{\mathrm{GA}}$ according to the following procedure.

Step 1 As the first generation ($\alpha = 1$), the initial population of $\boldsymbol{\rho}_{\mathrm{GA}}$ for N_{ind} individuals are randomly generated by the GA from a specified parameter search range.

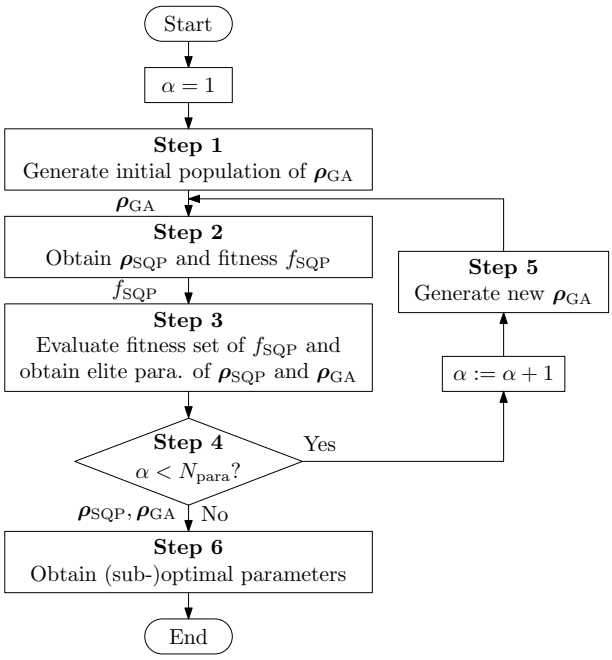

Fig. 2. Flowchart of the conventional autonomous design method.

Step 2 Under a constrained optimization problem, $\boldsymbol{\rho}_{\mathrm{SQP}}$ is optimized by the SQP and a fitness f_{SQP} is obtained for N_{ind} individuals of $\boldsymbol{\rho}_{\mathrm{GA}}$.

Step 3 The elite parameters of $\boldsymbol{\rho}_{\mathrm{SQP}}$ and $\boldsymbol{\rho}_{\mathrm{GA}}$ are obtained by evaluating the N_{ind} fitness values obtained in Step 2.

Step 4 If the number of generations α is less than the specified number N_{para}, set $\alpha := \alpha + 1$ and go to Step 5; otherwise, go to Step 6.

Step 5 For generating a new population, genetic operations such as selection, crossover, and mutation are performed by the GA. A series of procedure from Step 2 to Step 5 is repeated for N_{para} times.

Step 6 The elite parameters of $\boldsymbol{\rho}_{\mathrm{SQP}}$ and $\boldsymbol{\rho}_{\mathrm{GA}}$ at the N_{para}-th generation are adopted as the (sub)optimal parameters of $\boldsymbol{\Lambda}_C$.

In the following Sect. III-A2 and Sect. III-A3, the optimization problems used in Step 2 and Step 3 are briefly explained.

2) SQP-based Optimization Problem (Step 2): In the SQP-based optimization, the optimization problem of $\boldsymbol{\rho}_{\mathrm{SQP}}$ is defined as follows [11]:

$$f_{\mathrm{SQP}} = \min_{\boldsymbol{\rho}_{\mathrm{SQP}}} J_{\mathrm{obj}}(\boldsymbol{\rho}_{\mathrm{SQP}}) \text{ subject to } h_{\mathrm{sm}}(\boldsymbol{\rho}_{\mathrm{SQP}}) > r_{\mathrm{sm}}^2 \tag{9}$$

with

$$J_{\mathrm{obj}}(\boldsymbol{\rho}_{\mathrm{SQP}}) = \sum_{l=1}^{N_l} \left| L_{\mathrm{ds}}(j\Omega_l) - P(j\Omega_l)\boldsymbol{\Psi}_{\mathrm{GA}}(j\Omega_l)\boldsymbol{\rho}_{\mathrm{SQP}}^{\top} \right| \tag{10}$$

$$h_{\mathrm{sm}}(\boldsymbol{\rho}_{\mathrm{SQP}}) = \left| P(j\Omega_p)\boldsymbol{\Psi}_{\mathrm{GA}}(j\Omega_p)\boldsymbol{\rho}_{\mathrm{SQP}}^{\top} + \sigma_{\mathrm{sm}} \right|^2 \tag{11}$$

where $J_{\mathrm{obj}}(\boldsymbol{\rho}_{\mathrm{SQP}})$ is an objective function for expanding the control bandwidth, $h_{\mathrm{sm}}(\boldsymbol{\rho}_{\mathrm{SQP}})$ is a constraint inequality for ensuring the stability margins, and f_{SQP} is a fitness value.

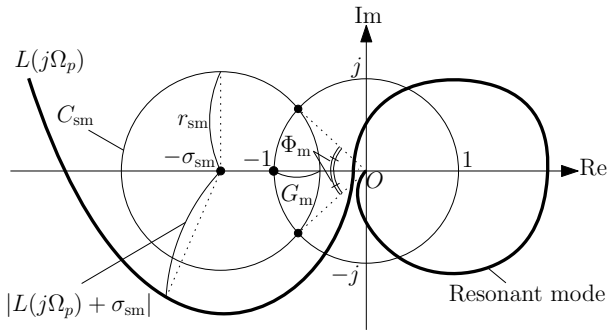

Fig. 3. Stability constraint on the Nyquist trajectory.

In (10), the objective function $J_{\rm obj}(\boldsymbol{\rho}_{\rm SQP})$ is the sum of distance between the desired open-loop characteristics $L_{\rm ds}(j\Omega_l)$ and the actual open-loop characteristics $P(j\Omega_l)\boldsymbol{\Psi}_{\rm GA}(j\Omega_l)\boldsymbol{\rho}_{\rm SQP}^{\top}$ at discrete frequencies $\Omega_l (l \in \{1,2,...,N_l\})$. Note that $L_{\rm ds}(j\Omega_l)$ are defined by the desired sensitivity characteristics $S_{\rm ds}(j\Omega_l)$ as

$$L_{\rm ds}(j\Omega_l) = \frac{1 - S_{\rm ds}(j\Omega_l)}{S_{\rm ds}(j\Omega_l)}. \tag{12}$$

The stability constraint $h_{\rm sm}(\boldsymbol{\rho}_{\rm SQP}) > r_{\rm sm}^2$ in (9) denotes that the Nyquist trajectory of the open-loop characteristics $L(j\Omega_p) := P(j\Omega_p)\boldsymbol{\Psi}_{\rm GA}(j\Omega_p)\boldsymbol{\rho}_{\rm SQP}^{\top}$ on the Nyquist diagram in Fig. 3 should pass through the outside of the circle $C_{\rm sm}$ defining the stability margins at the discrete frequencies $\Omega_p (p \in \{1,2,...,N_p\})$. The coordinate distance between $(-1, j0)$ and the intersection point of $C_{\rm sm}$ with the real axis denotes the gain margin $G_{\rm m}$ ($g_{\rm m} = 20\log_{10} G_{\rm m}$ [dB]), while the angle between the negative real axis and the vector from the origin to the intersection point of $C_{\rm sm}$ with a unit circle denotes the phase margin $\Phi_{\rm m}$ ($\phi_{\rm m} = 180\Phi_{\rm m}/\pi$ [deg]). The stability margins $g_{\rm m}$ [dB] and $\phi_{\rm m}$ [deg] are set by the center coordinates $(-\sigma_{\rm sm}, j0)$ of $C_{\rm sm}$ and the radius $r_{\rm sm}$ of $C_{\rm sm}$.

3) GA-based Optimization Problem (Step 3): In the GA-based optimization, the fitness values of $\boldsymbol{\rho}_{\rm GA}$ for $N_{\rm ind}$ individuals adopt the fitness values $f_{\rm SQP}$ obtained in Step 2. The optimization problem for $\boldsymbol{\rho}_{\rm GA}$ is defined as follows:

$$\min_{\boldsymbol{\rho}_{\rm GA}} \left\{ f_{\rm SQP}^{(1)}, f_{\rm SQP}^{(2)}, \cdots, f_{\rm SQP}^{(N_{\rm ind}-1)}, f_{\rm SQP}^{(N_{\rm ind})} \right\} \tag{13}$$

where the elite parameters of $\boldsymbol{\rho}_{\rm GA}$ are obtained by comparing $f_{\rm SQP}$ for $N_{\rm ind}$ individuals.

According to Sect. III-A2 and Sect. III-A3, a wide bandwidth FB controller with the specified stability margins will be designed by the optimization problems in (9) and (13). However, there is no guarantee that the FB controller achieves the time domain specifications (the settling time $T_{\rm set}$ and the settling accuracy $\pm\varepsilon$).

B. Time and Frequency Domain Optimization Method (Proposed)

The proposed method imposes a time domain optimization problem to reduce the tracking error e on the GA-based optimization problem, for realizing the time domain specifications.

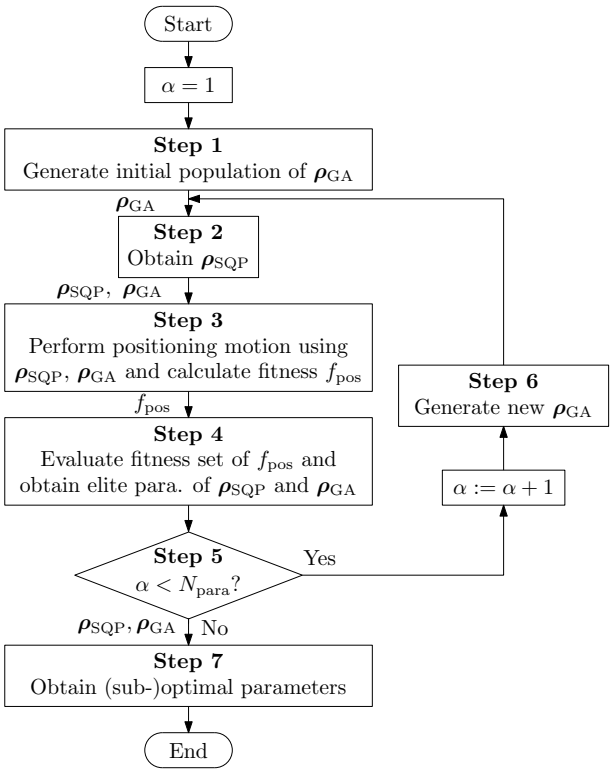

Fig. 4. Flowchart of the proposed design method.

1) Design Algorithm: Fig. 4 shows a flowchart of designing the controller parameters $\boldsymbol{\Lambda}_C$ based on the proposed autonomous design method. In the cooperative optimization method, the SQP optimizes $\boldsymbol{\rho}_{\rm SQP}$ for ensuring the stability margins, while the GA optimizes $\boldsymbol{\rho}_{\rm GA}$ for reducing the tracking error e. The detailed design procedure is shown as follows.

Step 1 As the first generation ($\alpha = 1$), the initial population of $\boldsymbol{\rho}_{\rm GA}$ for $N_{\rm ind}$ individuals are randomly generated by the GA from a specified parameter search range.

Step 2 To obtain stable PID gains $\boldsymbol{\rho}_{\rm SQP}$, the SQP optimizes $\boldsymbol{\rho}_{\rm SQP}$ under the constrained optimization problem (9) with $\boldsymbol{\rho}_{\rm GA}$ for $N_{\rm ind}$ individuals in the same way to the conventional method. Herein, although optimizing $J_{\rm obj}(\boldsymbol{\rho}_{\rm SQP})$ in (9) does not directly mean to reduce the tracking error e, $J_{\rm obj}(\boldsymbol{\rho}_{\rm SQP})$ is adopted for widening the control bandwidth.

Step 3 A positioning operation is performed by the obtained parameters $\boldsymbol{\rho}_{\rm SQP}$ and $\boldsymbol{\rho}_{\rm GA}$, and a fitness $f_{\rm pos}$ is obtained for $N_{\rm ind}$ individuals.

Step 4 The elite parameters of $\boldsymbol{\rho}_{\rm SQP}$ and $\boldsymbol{\rho}_{\rm GA}$ are obtained by evaluating the $N_{\rm ind}$ fitness values $f_{\rm pos}$ obtained in Step 4.

Step 5 If the number of generations α is less than the specified number $N_{\rm para}$, set $\alpha := \alpha + 1$ and go to Step 6; otherwise, go to Step 7.

Step 6 For generating a new population, genetic operations such as selection, crossover, and mutation are per-

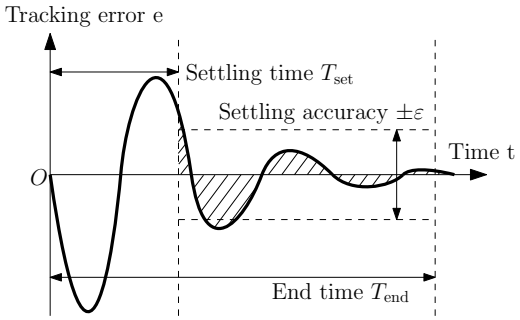

Fig. 5. Waveform of tracking error e.

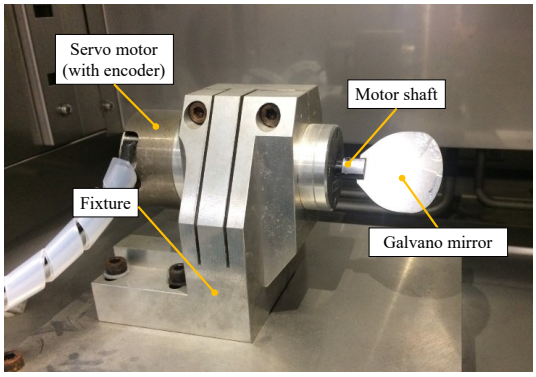

Fig. 6. Outside appearance of laboratory galvanometer scanner.

formed by the GA. A series of procedure from Step 2 to Step 6 is repeated for $N_{\rm para}$ times.

Step 7 The elite parameters of $\boldsymbol{\rho}_{\rm SQP}$ and $\boldsymbol{\rho}_{\rm GA}$ at the $N_{\rm para}$-th generation are adopted as the (sub)optimal parameters of $\boldsymbol{\Lambda}_C$.

In the following Sect. III-B2, the fitness $f_{\rm pos}$ and the optimization problem used in Step 4 are explained.

2) Optimization Problem for Reducing Tracking Error: Fig. 5 shows the waveform of the tracking error e. In Fig. 5, the fitness value $f_{\rm pos}$ is calculated by the sum of squares of e from the settling time $T_{\rm set}$ to the end time $T_{\rm end}$ as

$$f_{\rm pos} = \int_{T_{\rm set}}^{T_{\rm end}} \{e(t)\}^2 \, dt. \tag{14}$$

According to (14), the optimization problem for $\boldsymbol{\rho}_{\rm GA}$ is defined as

$$\min_{\boldsymbol{\rho}_{\rm GA}} \left\{ f_{\rm pos}^{(1)}, f_{\rm pos}^{(2)}, \cdots, f_{\rm pos}^{(N_{\rm ind}-1)}, f_{\rm pos}^{(N_{\rm ind})} \right\} \tag{15}$$

where the elite parameters of $\boldsymbol{\rho}_{\rm GA}$ are chosen by comparing $f_{\rm pos}$ for $N_{\rm ind}$ individuals. By introducing (15), it would be expected that e decreases within the settling accuracy $\pm\varepsilon$ as shown in Fig. 5.

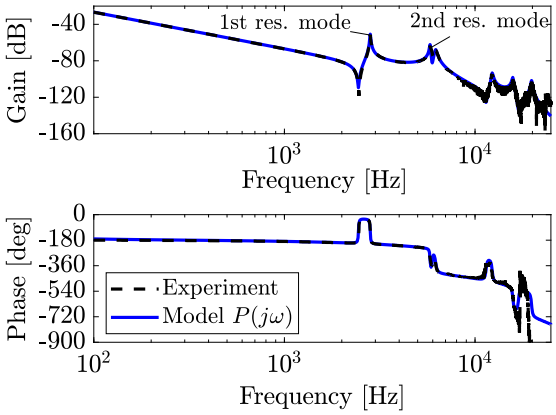

Fig. 7. Frequency characteristics of the plant.

IV. Simulation Evaluation of Autonomous Parameter Design Methods

A. Target Plant

Fig. 6 shows the outside appearance of a galvanometer scanner [12] for laser drilling of printed circuit boards that is a target plant for the evaluation of the proposed autonomous parameter design method. The galvanometer scanner is constituted by a galvano mirror equipped on the tip of the motor shaft, a servo motor, and an optical encoder detecting the motor angle. The laser beam on the printed circuit boards is irradiated to the desired position by controlling the motor angle.

In Fig. 7, the black dotted lines show the frequency characteristics of the plant experimentally measured from the motor current reference $i_{\rm ref}$ to the detected motor angle $\theta_{\rm m}$ by the sine sweep method. There are multiple mechanical resonance modes at frequencies above 2 kHz, where the first mode ($\omega_1 = 2\pi \times 2820$ rad/s) and second mode ($\omega_2 = 2\pi \times 5810$ rad/s) are caused by the torsion of the motor shaft and the deformation of the galvano mirror. These resonance modes deteriorate the control stability and positioning performance. Hence, the plant model from $i_{\rm ref}$ to $\theta_{\rm m}$ is defined as (16) considering six resonance modes:

$$P(s) = e^{-T_{\rm D}s} K_{\rm t} K_{\rm c} \sum_{\kappa=0}^{6} \frac{k_\kappa}{s^2 + 2\zeta_\kappa \omega_\kappa s + \omega_\kappa^2} \tag{16}$$

where $T_{\rm D}$ is the equivalent dead time, $K_{\rm t}$ is the torque constant of the motor, $K_{\rm c}$ is the total gain of the moment of inertia and the current control system, ζ_κ is the κ-th mode damping coefficient, ω_κ is the κ-th mode frequency, k_κ is the κ-th mode gain. In Fig. 7, the blue lines show the frequency characteristics of the manually identified model of $P(j\omega)$.

B. Target Control Specifications

For the 2-DoF position tracking control of the galvanometer scanner, in the block diagram of Fig. 1, the FF control input $u_{\rm FF}$ and the reference r as the target position trajectory are

TABLE I
PARAMETERS OF THE DESIRED SENSITIVITY $S_{\rm ds}(s)$.

$K_{\rm s}$	$\omega_{\rm s1}$ [rad/s]	$\zeta_{\rm s2}$	$\omega_{\rm s2}$ [rad/s]
1.0	$2\pi \times 300$	0.6	$2\pi \times 600$

TABLE II
SETTINGS OF GENETIC OPERATION.

Number of generations $N_{\rm para}$	100
Number of individuals $N_{\rm ind}$	10
Selection rate	1.00
Crossover rate	0.99
Mutation rate	0.08

designed by the final state control manner [13] considering $P(s)$, and the controlled output y ($\propto \theta_{\rm m}$) is defined as the equivalent linear motor position corresponding to the laser position. The target position trajectory r is specified as a stroke of 1 mm and a settling time of $T_{\rm set} = 0.72$ ms. In addition, the target settling accuracy of e is specified as $\varepsilon = 2$ μm or less after the settling time. Finally, for stabilizing the FB control system, a gain margin and a phase margin are respectively specified as $g_{\rm m} = 5$ dB and $\phi_{\rm m} = 30$ deg, and the first and second resonance modes are stabilized by the gain/phase stabilization method to realize the positioning specification.

C. Setting of Autonomous Parameter Design

First, according to Sect. IV-B, the target cascade structure FB controller has a PID compensator and two all-pass filters ($N_{\rm A} = 2$) for stabilizing the first and second resonance modes as follows:

$$C(s) = C_{\rm PID}(s) C^{(1)}_{\rm APF}(s) C^{(2)}_{\rm APF}(s) \tag{17}$$

where the controller parameters $\boldsymbol{\Lambda}_C$ to be designed are defined as follows:

$$\boldsymbol{\Lambda}_C = \left[K_{\rm P}\ K_{\rm I}\ K_{\rm D}\ \tau_{\rm D}\ \zeta_{\rm A1}\ \zeta_{\rm A2}\ \omega_{\rm A1}\ \omega_{\rm A2}\right]. \tag{18}$$

Second, the desired sensitivity characteristic $S_{\rm ds}(s)$ is designed as the following high-pass filter:

$$S_{\rm ds}(s) = \frac{K_{\rm s} s^3}{(s+\omega_{\rm s1})(s^2 + 2\zeta_{\rm s2}\omega_{\rm s2} s + \omega_{\rm s2}^2)} \tag{19}$$

where $K_{\rm s}$, $\omega_{\rm s1}$, $\zeta_{\rm s2}$, and $\omega_{\rm s2}$ are setting parameters. The parameters are assigned as in Table I so that the desired control bandwidth becomes about 1 kHz. For the detail of the design of $S_{\rm ds}(s)$, see [11]. For calculating the objective function $J_{\rm obj}$, the discrete frequencies Ω_l are imposed at $\Omega_l = 2\pi \times \{100, 109, 118, \cdots, 1000\}$ rad/s ($N_l = 101$).

Third, according to the gain margin of $g_{\rm m} = 5$ dB and the phase margin of $\phi_{\rm m} = 30$ deg, $\sigma_{\rm sm} = 1.13$ and $r_{\rm sm} = 0.56$ are set for the stability constraint. For calculating the stability constraint $h_{\rm sm}$, the discrete frequencies Ω_p are imposed at $\Omega_p = 2\pi \times \{10, 15, 20, \cdots, 25000\}$ rad/s ($N_p = 4999$).

Finally, for the GA-based optimization, the genetic operation is listed in Table II and the parameter search range of $\boldsymbol{\rho}_{\rm GA}$ is listed in Table III, while the end time $T_{\rm end}$ is defined as $T_{\rm end} = 3.0$ ms for calculating the fitness value $f_{\rm pos}$.

TABLE III
PARAMETER SEARCH RANGE OF $\boldsymbol{\rho}_{\rm GA}$ IN THE GA.

Parameter	Minimum	Maximum
$\tau_{\rm D}$ [s]	6.37×10^{-6}	1.59×10^{-4}
$\zeta_{\rm A1}$	1.0×10^{-3}	1.0
$\zeta_{\rm A2}$	1.0×10^{-3}	1.0
$\omega_{\rm A1}$ [rad/s]	$2\pi \times 2000$	$2\pi \times 3000$
$\omega_{\rm A2}$ [rad/s]	$2\pi \times 5000$	$2\pi \times 9000$

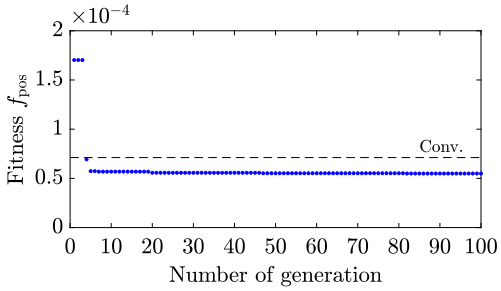

Fig. 8. Fitness value $f_{\rm pos}$.

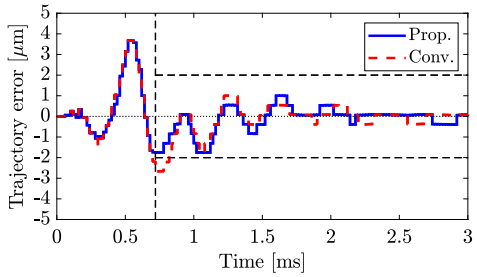

Fig. 9. Waveforms of position error e.

D. Design Results

The autonomous parameter design is performed by the proposed and conventional methods. In this study, a positioning simulation is performed with the plant parameter variation (the torque constant K_t: -0.1 %, the 1st resonant frequency ω_1: $-2\pi \times 50$ rad/s, and the 2nd resonant frequency ω_2: $-2\pi \times 100$ rad/s) as modeling errors on the FF design. Fig. 8 shows elite fitness values of $f_{\rm pos}$ for generations of the GA in the proposed method, while Fig. 9 shows the tracking error e. In Fig. 8, a black dotted line shows a fitness value obtained by the FB controller designed by the conventional method. By comparing the fitness values, the proposed method decreases $f_{\rm pos}$ less than the conventional method at the last generation. As a result, in Fig. 9, the FB controller designed by the proposed method could achieve the better positioning performance than the conventional method, successfully satisfying the target settling accuracy of ± 2 μm.

Figs. 10–13 show frequency characteristics of the FB control systems designed by both methods. From the open-loop characteristics and Nyquist diagram of Figs. 11–12, both methods ensure the desired stability margin. However, the loop shaping properties of both methods are slightly different, owing to the time domain optimization of the proposed method.

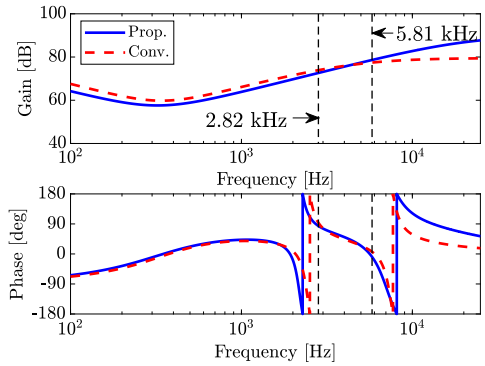

Fig. 10. FB controller $C(j\omega)$.

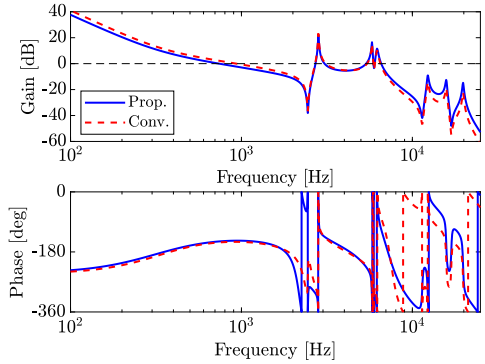

Fig. 11. Open-loop characteristics $L(j\omega)$.

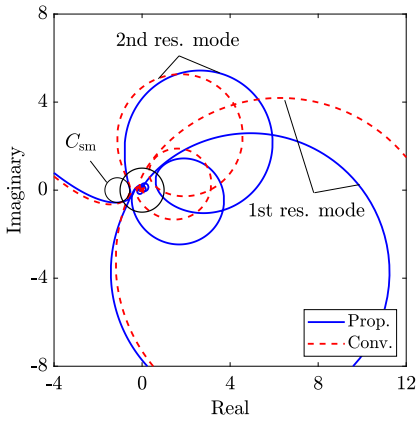

Fig. 12. Nyquist diagram of $L(j\omega)$.

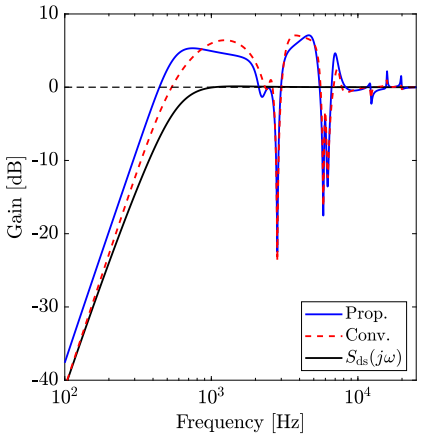

Fig. 13. Sensitivity characteristics $S(j\omega)$.

V. Conclusion

In this paper, an autonomous parameter design method for a cascade structure FB controller that considers both time and frequency domain properties is presented. In the proposed method, a cooperative optimization method could design the parameters that improved the positioning performance in time domain while ensuring the specified stability margins as well as a wide bandwidth in frequency domain, comparing to the conventional method.

Acknowledgment

The authors would like to thank Via Mechanics, Ltd, for providing the experimental equipment.

References

[1] M. Kobayashi, S. Nakagawa, T. Atsumi, and T. Yamaguchi, "High-bandwidth servo control designs for magnetic disk drives," in *Proc. 2001 IEEE/ASME Int. Conf. Adv. Intell. Mechatronics*, pp. 1124–1129, 2001.

[2] M. Iwasaki, K. Seki, and Y. Maeda, "High-precision motion control techniques: a promising approach to improving motion performance," *IEEE Ind. Electron. Mag.*, vol. 6, no. 1, pp. 32–40, 2012.

[3] T. Atsumi and W. C. Messner, "Modified bode plots for robust performance in SISO systems with structured and unstructured uncertainties," *IEEE Trans. Control Syst. Technol.*, vol. 20, no. 2, pp. 356–368, 2012.

[4] N. Hirose, M. Iwasaki, M. Kawafuku, and H. Hirai, "Robust vibration suppression of resonant modes by feedback compensation realized using allpass filters," (in Japanese), *IEEJ Trans. Ind. App.*, vol. 129, no. 10, pp. 981–988, 2009.

[5] Y. Maeda, E. Kuroda, T. Uchizono, and M. Iwasaki, "Hybrid optimization method for high-performance cascade structure feedback controller design," in *Proc. 44th Annu. Conf. IEEE Ind. Electron. Soc.*, pp. 4588–4593, 2018.

[6] R. Kitayoshi and H. Fujimoto, "Automatic adjustment method of controller structure and parameter based on structured H∞ control," in *Proc. 45th Annu. Conf. IEEE Ind. Electron. Soc.*, pp. 3263–3268, 2019.

[7] P. Gahinet and P. Apkarian, "Structured H_∞ synthesis in MATLAB," in *Proc. 18th IFAC World Congr.*, pp. 1435–1440, 2011.

[8] A. Nath and S. Kaitwanidvilai, "High performance HDD servo system using GA based fixed structure robust loop shaping control," in *Proc. 2009 IEEE Int. Conf. Robot. Biomimetics*, pp. 1854–1859, 2009.

[9] M. Yamamoto, Y. Okitsu, and M. Iwasaki, "GA-based auto-tuning of vibration suppression controller for positioning devices with strain wave gearings," in *Proc. 2015 IEEE Int. Conf. Mechatron.*, pp. 614–619, 2015.

[10] S. Ibaraki, T. Tanaka, A. Matsubara, and Y. Kakino, "A numerical optimization approach to frequency-domain loop-shaping design of a fixed-structure controller (design of an anti-vibration filter for a feed drive system)," (in Japanese), *Trans. the Japan Soc. Mechanical engineer Ser. C*, vol. 70, no. 691, pp. 687–692, 2004.

[11] E. Kuroda, Y. Maeda, and M. Iwasaki, "Autonomous parameter design for cascade-structure feedback controller based on cooperative optimization method," *IEEJ J. Ind. App.*, vol. 10, no. 4, pp. 457–468, 2021.

[12] Y. Maeda and M. Iwasaki, "Circle condition-based PID controller design considering robust stability against plant perturbations," in *Proc. 39th Annu. Conf. IEEE Ind. Electron. Soc.*, pp. 6442–6447, 2013.

[13] M. Hirata and F. Ueno, "Final-state control using polynominal and time-series data," *IEEE Trans. Magn.*, vol. 47, no. 7, pp. 1944–1950, 2011.